Theoretical Study on the Stability of Low-Spin Hydridomethyl Complexes of the First-Row Transition Metal Cations

M. Hendrickx,* M. Ceulemans, K. Gong, and L. Vanquickenborne

Department of Chemistry, University of Leuven, Celestijnenlaan 200F, B-3001 Heverlee-leuven, Belgium

Received: September 9, 1996; In Final Form: January 22, 1997[⊗]

Theoretical calculations have been performed in order to study the stability of the low-spin hydridomethyl complexes $HMCH_3^+$ for the first-row transition metals ($M^+ = Sc^+-Cu^+$). Originally experimental results have been rationalized by assuming a low-spin hydridomethyl complex as a stable intermediate in the reactions of methane with singly charged metal cations. Recently, theoretical studies showed that for some late transition metals of the first row (Fe^+ and Co^+) no stable low-spin insertion product could be located on the potential energy surface. For the early elements of this row (Sc^+-V^+) the experimental cross section ratios $\sigma(MH^+)/\sigma(MCH_3^+)$ indicate that the elimination reactions for these cations proceed via a statistically behaved intermediate. Our CASPT2 calculations indeed confirm a stable hydridomethyl complex for these cations. The reason for the stability of the insertion complexes could be traced back to the relative position of the lowest lying low-spin s^0d^n state and the lowest lying low-spin s^1d^{n-1} state in the electronic spectrum of the corresponding free transition metal cations. Further, an analysis of the wave function clearly reveals a correlation between the extent of the participation of the 4s orbital in the metal−ligand bonds and the experimentally observed dominance of the H_2 elimination over the other elimination reactions for the cations Sc^+ to Cr^+. An explanation in terms of the frontier orbital approach is given.

Introduction

Gas phase reactions of the singly charged first-row transition metal cations (M^+) with methane have been the subject of intensive experimental research. On the basis of several guided-ion-beam studies the following periodic trend for this particular branch of gas phase chemistry was observed. For the three elimination reactions (1)-(3), which are all detected for the first-row transition metals,[1] the branching ratios were noticed to vary across the periodic table.

$$M^+ + CH_4 \rightarrow MCH_3^+ + H \quad (1)$$

$$\rightarrow MCH_2^+ + H_2 \quad (2)$$

$$\rightarrow MH^+ + CH_3 \quad (3)$$

For the early metals such as Sc^+, Ti^+, V^+, and Cr^+, the H_2 elimination (reaction 2) appears to be the major process at low kinetic energies of the cation, whereas at elevated energies the methyl elimination process (reaction 3) becomes dominant. For late metals on the other hand, the latter process is always dominant. All three elimination processes are endothermic for all first-row transition metal cations, the H_2 elimination however being energetically considerably more favorable.

Furthermore, guided-ion-beam experiments have proven to be particularly suited for exploring the effect of the electronic state of the cations on their reactivity. Combining the results for the different metal cations led to the formulation of two rules that control the reactivity of a specific term.[1] The first rule, also known as the symmetry rule, states that an efficient reaction can only be expected for electronic terms originating from an s^0d^n configuration. The second rule on the other hand (spin conservation rule) places a restriction on the spin multiplicity of the metal: only low-spin states are observed to react efficiently. Both rules can be understood by assuming an oxidative addition of the metal cation into a C−H bond of methane to be the first step in all observed reactions. This results in the formation of hydridomethyl insertion complexes ($HMCH_3^+$), which are believed to constitute a minimum on the potential energy surface. The presence of two M−L σ bonding orbitals is supposed to give rise to a low-spin ground state for the insertion complexes. Each bonding orbital is occupied by two electrons, which formally can be seen as the outcome of the pairing of two metal electrons with two electrons originally occupying the C−H bonding orbital. The symmetry rule follows from the repulsive interaction between the 4s orbital of the cation and the σ C−H bonding orbital of methane. During the early stages of the insertion reaction this leads to a destabilization of all states characterized by an occupation of the 4s orbital.

Due to the complex nature of the electronic structure (near degeneracy effects) of the molecular structures involved in these elimination reactions, the number of theoretical investigations is rather limited. Only recently detailed calculations on reactions 1−3 for Co^+ and Fe^+ have been studied by Musaev et al. at the MR-SDCI-CASSCF level of approximation.[2,3] In agreement with our CASPT2 study [4] of the oxidative addition reactions of Co^+ to a C−H bond of methane, ethane, and propane, these authors could not locate a stable low-spin $HMCH_3^+$ structure on the potential energy surface. A similar result was reached by a B3LYP study for the Fe^+/C_2H_6 system.[5] On the quartet surface a $HFeC_2H_5^+$ structure was found to be separated from the reactants by an energy barrier of only 1 kcal/mol. The only calculated insertion complex with sufficient stability, so far, is a high-spin (quintet) linear structure of $HCoCH_3^+$.[4] As this complex correlates with the ^5F (s^1d^7) state of Co^+, a substantial energy barrier was found in the entrance channel, which leads to the prediction of an inefficient reaction for this specific term. All the theoretical studies mentioned consider the low-spin hydridoalkyl structure as a precursor for the different elimination reactions.

[⊗] Abstract published in *Advance ACS Abstracts,* March 1, 1997.

S1089-5639(96)02754-5 CCC: $14.00

The most direct experimental evidence for a sufficient stable $HMCH_3^+$ intermediate has been given for vanadium.[6] For the reaction of V^+ with 2-methylpropane and 2,2-dimethylpropane a particle corresponding to the stoichiometry of VCH_4^+ was detected in the mass spectrometer. Because this particle was measured to be endothermic with respect to $V^+ + CH_4$, an electrostatic adduct structure was ruled out and the hydridomethyl structure proposed. The aim of the present contribution is to investigate the stability of the low-spin hydridomethyl complexes of the first-row transition metal cations Sc^+ to Cu^+. For this purpose we have performed CASPT2 calculations on the low-spin hydridomethyl complexes for the first-row transition metal cations from Sc^+ to Cu^+. Obviously, a statement about the stability of the intermediates can only be made when also the transition states leading from the adducts to the insertion complexes have been located on the potential energy surface. In discussing our results we will pay special attention to the trends that can be observed across the periodic table, rather than to quantitative energetic results. This strategy has proven to be notably successful for uncovering the underlying principles controlling the reactivity of the second-row transition metal cations with methane.[7]

Computational Details

The CASSCF method combined with gradient techniques has been used to optimize the geometry of the insertion complexes. The active space used was chosen to incorporate the most relevant near degeneracy effects. An analysis of the CASSCF wave function of the various conformations of $HCoCH_3^+$ in our previous calculations clearly revealed the presence of not only a cluster of four nonbonding metal d orbitals but also a significant population of the Co−C antibonding orbital. Therefore in our geometry optimization, we have used an active space that includes—besides these nonbonding orbitals—also the bonding−antibonding pair of orbitals for both M−L interactions. This amounts to a total of eight active orbitals. An exception was made for the copper cation, for which the nonbonding orbitals are all fully occupied by two electrons, so that no degeneracy effects can be expected from them. The resulting active space reduces to four orbitals describing the bonding and antibonding effects for the Cu−H and Cu−C bonds. During these geometry optimizations of the minima on the potential energy surface a C_s symmetry was imposed. From our previous study and from other calculations for this kind of molecule we can trust this restriction to be completely acceptable and even to be without any extra significant error.[2,3,5]

Transition states were located by applying the coordinate-driven method. This was achieved by selecting the H−M−C angle as the driving coordinate. Again a C_s symmetry was presumed. To check the selection of the H−M−C angle as the driving coordinate, a full gradient transition state determination was performed for the insertion of Ti^+. No symmetry restrictions were imposed, which at the same time enables us to make an assessment of the symmetry restriction that we have imposed. In addition a frequency analysis will be carried out on the transition state as well as on the insertion complex of this complex.

For energy calculations also the dynamical correlation effects have to be incorporated. This is done by performing CASPT2 calculations on the CASSCF structures.[8,9] Recent experience on transition metal complexes has shown that good results for binding energies can be expected when the double-shell effect is accounted for in the choice of the active space.[10] For the hydridomethyl complexes this means that the active space used in the geometry optimization has to be enlarged by four 3d' orbitals, each one corresponding to an orbital from the cluster of the nonbonding 3d orbitals. This gives us an active space that includes 12 orbitals. In all CASPT2 calculations only the 1s, 2s, and 2p of the metal and the 1s electrons of carbon are excluded from the correlation treatment. Final binding energies were obtained by taking into account relativistic corrections (first-order perturbation theory applied to compute mass velocity and Darwin contributions to the total energies), basis set superposition error (estimated by the counterpoise method), and zero-point vibrational energy (calculated from a frequency analysis at the CASSCF level).

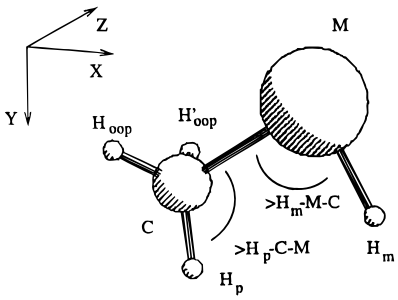

Figure 1. Definition of the coordinate system and the internal coordinates. The *xy* plane contains the atoms H_m, M^+, C, and H_p.

For the localization of the reaction path and the equilibrium structures an ANO basis set consisting of a (17s,12p,9d,4f/6s,4p,3d,1f) set for the metal cations, a (10s,6p,3d/4s,3p,1d) set for carbon, and a (7s,3p/3s,1p) set for hydrogen was used.[11] All these calculations were carried out using the MOLCAS3 quantum chemical software.[12] The full gradient search for the transition state on the Ti^+/CH_4 potential energy surface was carried out by using the GAMESS program.[13] In this calculation it is more appropriate to use a segmented basis set. A modified Wachters basis (17s,14p,6d/9s,6p,4d)[14] for the transition metal cations and a Huzinaga−Dunning set for carbon (9s,4p/4s,2p) and hydrogen (4s/3s) were chosen.[15]

Results and Discussion

Geometric and Electronic Structure. The coordinate system used in our calculations and the definition of the internal coordinates for the complexes are shown in Figure 1. As shown in the figure, we carried out calculations on the eclipsed conformations of the transition states and of the equilibrium geometries. Previous theoretical studies on $HFeCH_3^+$ and $HCoCH_3^+$ have shown that there is essentially a free rotation around the M−C bond.[2,3,5] The energy difference between the eclipsed and staggered conformation, as well as the energy barrier separating them, was found to be less than 1 kcal/mol. The former conformation appeared to be the most stable structure. It should be stressed that this result was reached by carrying out geometry optimization without any symmetry restrictions. All these findings indicate that imposing an eclipsed conformation in our optimizations of the insertion complexes can be considered as being quite acceptable. Imposing an eclipsed structure can easily be done by fixing the dihedral angle $H_m-M-C-H_p$ to 0° and by leaving all other internal coordinates free to adapt themselves.

The results of these optimizations for the CASSCF *equilibrium structures* are collected in Table 1. As can be expected, the M−H distances decrease from the left of the row to the right, reflecting the decrease of the ionic radius of the free metal cations. If we compare these distances with the results calculated by the generalized valence bond (GVB) method for the metal hydrides $M-H^+$,[16] we find a very good resemblance, the differences being always smaller than 0.06 Å. The M−C distances on the other hand should be comparable with those calculated by Bauschlicher et al. in their MCPF studies of the

TABLE 1: Geometries for the Equilibrium Structures of the Hydridomethyl Complexes Calculated at the CASSCF Level:[a] Occupation Numbers of the Natural Orbitals Representing the M−C and M−H Bonding Orbital

	$Sc^+ {}^1A'$	$Ti^+ {}^2A''$	$V^+ {}^3A'$	$Cr^+ {}^4A'$	$Mn^+ {}^5A'$	$Fe^+ {}^4A''$	$Co^+ {}^3A''$	$Ni^+ {}^2A'$	$Cu^+ {}^1A'$
M−C (Å) this work	2.14	2.10	2.15	2.54	2.38	2.27	2.13	2.07	2.00
ref 18	2.13	2.06	2.02	1.99	2.03	1.97	1.99	1.89	1.98
M−H (Å) this work	1.78	1.73	1.69	1.66	1.73	1.67	1.60	1.55	1.50
ref 16	1.81	1.73	1.66	1.60	1.70	1.65	1.61	1.56	1.51
$\angle H_m-M-C$ (deg)	109.4	112.3	105.0	126.9	114.3	111.2	93.6	94.3	84.6
$\angle H_p-C-M$ (deg)	109.5	104.5	104.8	94.9	102.5	103.2	109.6	108.9	113.3
occ σ(M−C)[a]	1.93	1.88	1.77	1.34	1.37	1.40	1.58	1.66	1.86
occ σ(M−H)[a]	1.95	1.95	1.94	1.95	1.92	1.93	1.99	1.99	1.95

singly charged metal methyls and dimethyls[17,18] and with the DFT and QCISD(T) study of the monomethyl complexes by Holthausen et al.[19] These previous studies all fairly well agree among each other on the calculated M−C bond distance. The deviations between them are smaller than 0.01 Å. Consequently, for the sake of comparison with our CASSCF results it is sufficient to include only the MCPF results for $M(CH_3)_2^+$ in Table 1. Inspection of Table 1 leads to the following conclusions. Good resemblance is found at the left side and the far right side of the row. Poor agreement, on the other hand, is obtained for Cr^+ to Ni^+, the difference being the largest for Cr^+, for which it amounts to as much as 0.55 Å. It should however be mentioned that for this insertion complex the potential energy surface is extremely flat in the equilibrium region, and changing the M−C distance by 0.55 Å shows only a minor effect on the total energy of the molecule.

As is the case for the M−H distances and MCPF results of Bauschlicher et al.,[17,18] we would expect the M−C distance to decrease from the left to the right across the row. Our CASSCF values deviate from this behavior in the sense that for the early metals the bond length remains more or less constant for Sc^+, Ti^+, and V^+, then dramatically increases for Cr^+, and finally from this cation onward decreases. In particular the large increase of the M−C bond for Cr^+ and the pronounced strong shortening of this bond for the late cations are notably different from the observed trends for the M−C bond distance in the previous single-reference calculations[17−19]. On the basis of these observations we must conclude that the evolution of the ionic radius of the cation across the first row cannot possibly be responsible for the behavior of the M−C bond, and therefore covalent effects must be considered. In order to do so the occupation numbers of the M−C bonding orbital are also given in Table 1. The occupation of the corresponding antibonding orbital can be obtained by simply subtracting the occupation number of the bonding orbital from 2. For the first three cations the population of M−C bonding orbital declines from Sc^+ to V^+, indicating a weakening of the M−C bond. As this trend opposes the evolution of the ionic radius, a roughly constant M−C bond length is not unreasonable. Furthermore, the large increase in bond length for Cr^+ and Mn^+ is indeed reflected in the large reduction of the occupation of the M−C bonding orbital and the simultaneous increase of the population in the corresponding antibonding orbital. The occupation numbers of the M−H bonding orbitals are also given in Table 1. These values remain more or less constant at 2 across the row, pointing to the fact that the M−H bonding is not affected and therefore explaining the gradual decline of the M−H bond distance due to ionic effects.

The deviations between the CASSCF and the MCPF calculated M−C bond distances closely follow the divergence of the occupation number of the M−C bonding orbital from 2. Indeed, the largest differences are found in the middle of the row (Cr^+, Mn^+, Fe^+), whereas almost perfect agreement between our multireference study and previous single-reference studies was reached for those cations where the occupation number of the M−C bonding orbital only slightly varies from 2. The CASSCF bond distances are always calculated to be larger due to the depopulation of the bonding orbital and the simultaneous population of the corresponding antibonding orbital. We can therefore conclude that near degeneracy effects are of great importance in the present investigation. In the previous studies on $M(CH_3)^+$ and $M(CH_3)_2^+$ complexes only single-reference methods were used. It is therefore quite reasonable that large deviations in the M−C bond distances can be expected. As can be seen in Table 1 this is the case in the middle of the row, where the contribution of the antibonding M−C orbital to the electronic structure is not negligible.

TABLE 2: Results of a Mulliken Population analysis of the CASSCF Wave Functions of the Insertion Products and the Transition States: Charges on the Metal (Q(M)) and the Methyl Group ($Q(CH_3)$) Are Given for the Insertion Product

	Sc^+	Ti^+	V^+	Cr^+	Mn^+	Fe^+	Co^+	Ni^+	Cu^+
Insertion Product									
4s	0.55	0.49	0.56	0.46	0.83	0.82	0.78	0.76	0.61
3d	1.08	2.25	3.24	4.41	5.11	6.14	7.20	8.25	9.46
Q(M)	1.10	1.00	1.05	0.97	0.92	0.88	0.88	0.84	0.78
$Q(CH_3)$	−0.03	0.06	0.07	0.17	0.18	0.20	0.19	0.20	0.24
Transition State									
4s	0.39	0.32	0.26	0.25	0.64	0.39	0.45	0.53	0.49
3d	1.45	2.54	3.55	4.60	5.22	6.52	7.50	8.41	9.63

The evolution of the $M-C-H_p$ angle is also given in Table 1. Again our results can be compared with the MCPF results found for the monomethyls and the dimethyls. For both types of complexes the MCPF calculations found this angle to decrease monotonously from the left of the row to the right. For instance for the dimethyl complexes this angle varies from about 111° for $Sc(CH_3)_2^+$ to about 90° for $Cu(CH_3)_2^+$. This evolution was ascribed to the charge donation from the methyl ligand to the metal cation, which is the largest for the late metals, and to the fact that calculations for CH_3 and CH_3^+ indicate that the latter ionic structure more strongly prefers a planar structure. Our values for this angle exhibit a different trend across the row. They first decrease to reach a minimum for Cr^+ and increase again. As a population analysis of the CASSCF wave functions (Table 2) does indeed reveal larger donation effects for the late metal cations (as suggested from the MCPF studies), we must conclude that another factor has a greater impact on the $M-C-H_p$ angle. A close inspection of table 1 shows a rather strong correlation between this angle and the M−C distance: the larger the bond length the smaller the angle. The underlying effect determining the $M-C-H_p$ bond angle should therefore be assigned to a repulsive interaction between the electrons occupying the nonbonding metal orbitals and the C−H bonds in the ligand, which causes the methyl group to bend away from the cation.

The geometries for the *transition states* as they were determined on the CASSCF potential energy surface by the coordinate-driven method are collected in Table 3. The transition state was located only for the state that gives the most stable insertion product. For all complexes where a low lying excited state could be expected (due to the degeneracy of the nonbonding d orbitals) this state was calculated at several points

TABLE 3: Geometries for the Transition States Optimized at the CASSCF Level

	Sc^+	Ti^+	V^+	Cr^+	Mn^+	Fe^+	Co^+	Ni^+	Cu^+
M−C (Å)	2.01	2.10	2.11	2.13	2.41	2.03	2.01	1.97	1.94
M−H (Å)	1.81	1.66	1.69	1.65	1.67	1.57	1.56	1.48	1.46
$\angle H_m-M-C$ (deg)	51.1	49.8	50.6	51.5	56.1	55.3	60.5	85.8	79.3
$\angle H_p-C-M$ (deg)	154.4	142.7	140.4	135.8	113.0	130.6	130.5	117.0	113.6

of the potential energy surface. In all cases it was found that the energy differences from the state corresponding to the ground state of the insertion complex are smaller than 5 kcal/mol. With respect to the accuracy of our CASPT2 calculations and the fact that we are not pursuing quantitative energetic results, we can confine ourselves to the ground state in our discussion As was mentioned in the Introduction, an eclipsed C_s geometry was imposed in our survey of the potential energy surface. To check if this restriction does not cause any anomalies, we conducted a full gradient search of the transition state for the insertion of Ti^+ into a C−H bond. This resulted in a transition state with a dihedral angle $H_m-M-C-H_p$ that amounts to only 13°. For this geometry we carried out a CASPT2 calculation using the same basis and active space as used for the calculation of the energetics of the C_s structures. Since a difference of only 1.5 kcal/mol was obtained, it is safe to state that imposing a C_s symmetry for the location of the transition states introduces an error that falls well within the accuracy of our calculations. This does not come as a surprise. Indeed, as was mentioned earlier in this paper and in the literature,[2−4] the structures at hand (including the transition states) are characterized by a free rotation around the M−C bond. Hence we feel comfortable that imposing a C_s symmetry will not jeopardize the qualitative conclusions that we will draw in the next sections.

If we compare the bond distances M−C and M−H given in Table 3 with those of the corresponding insertion complexes in Table 1, it is immediately clear that both metal ligand bonds are already completely formed in the transition states. Actually, the bond length in the transition states is in most cases somewhat shorter than in the insertion complexes. This can be attributed to the difference in electronic structure between the TS and the insertion complex. The former is better described as corresponding to the s^0d^n configuration, whereas the latter is characterized by an increase of the 4s population (Table 2). Consequently, for a particular cation the hydridomethyl complex resembles more the s^1d^{n-1} configuration than the corresponding transition state. In fact the transition states are reached where the low-spin s^0d^n diabatic surface (s^0 facilitates C−H insertion) crosses the s^1d^n diabatic surface (see below). The smaller radial extent of the 3d shell (as compared to the 4s orbital), which is especially true for the late transition metals, explains the observed shorter M−L distances in the transition states. Additional information about the strength of the two metal ligand bonds can be gathered from a vibration analysis. For the Ti^+ insertion the diagonalization of the Hessian matrix computed for the transition state structure (which gives only one negative eigenvalue) results in a zero-point energy correction of 4.9 kcal/mol with respect to the reactants Ti^+ and CH_4. A vibrational analysis on the stable insertion complex $HTiCH_3^+$ gives nearly the same value of 4.7 kcal/mol, indicating that both structures have similar binding energies. The H_m-M-C angle (Table 3), which was used as the driving coordinate for the localization of the transition states, gives us a first clue on the stability of the insertion complexes. For most cations a value was obtained lying between 50° and 60°, Ni^+ and Cu^+ being however exceptions. For these cations the H_m-M-C angles in the transition state and insertion complex do not differ much. Actually, both structures resemble each other very well, questioning the stability of the insertion complexes of both cations with respect to the dissociation into M^+ and CH_4.

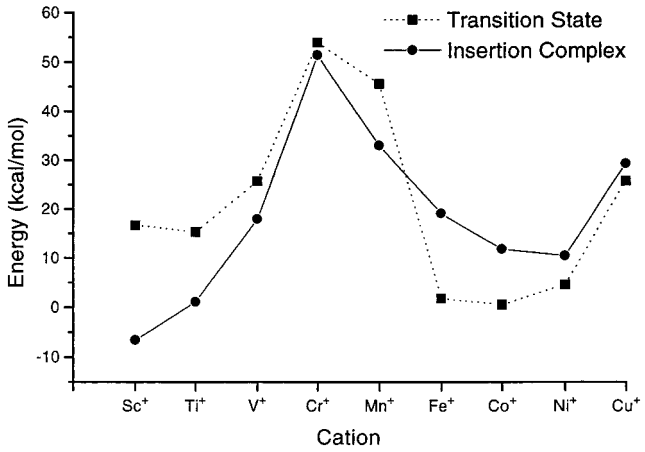

Figure 2. Relative energies (kcal/mol) for the insertion products and the transition states with respect to the ground state asymptote ($M^+ + CH_4$). Energies calculated at the CASPT2 level and corrected for zero-point vibrational energy, basis set superposition error, and relativistic effects.

Binding Energies. CASPT2 energies were calculated at the CASSCF geometries and corrected for zero-point vibrational energies, basis set superposition errors (ranging from 5 to 11 kcal/mol as estimated by the counterpoise method), and relativistic effects. Binding energies are expressed relative to the ground state of the different metal cations, which have been calculated with 3d, 4s, and 3d′ active space. The total electronic energy of methane was calculated by the MP2 method. The number of electrons correlated in free metal cations and methane corresponds to the number of electrons correlated in the complex structures. The resulting binding energies that were obtained from these calculations are collected in Table 4 and are graphically depicted in Figure 2. Negative values correspond to energies that are situated below the ground state asymptote of the $M^+ + CH_4$ system. The general shapes of both curves agree well with the findings for the second-row transition metal complexes.[7] The curve for the insertion complexes (full line in Figure 2) has a maximum at Cr^+ and Cu^+. Only $HScCH_3^+$ appears to be exothermic, whereas $HTiCH_3^+$ is thermoneutral. All other insertion products are situated well above the ground state asymptote. The position of the barrier heights, which is represented in Figure 2 as a dashed line, follows more or less the same trend as the binding energy of the insertion products (full line). Both lines cross each other however between Mn^+ and Fe^+. Consequently, from Fe^+ to Cu^+ the transition states are located lower in energy than the insertion complexes. For these cations the CASSCF minimum disappears at the CASPT2 level. A similar conclusion was reached by Musaev et al. for Fe^+ and Co^+.[2,3] Stable intermediates are predicted for Sc^+, Ti^+, V^+, and Mn^+. For Cr^+ the transition state and insertion complex have more or less the same energy, the latter structure being somewhat more stable. As mentioned previously, the potential energy surface is extremely flat in the neighborhood of the $HCrCH_3^+$, making it a very short-living intermediate.

The obtained results show that for the early transition metal cations the CASSCF and CASPT2 potential energy surfaces are quite parallel. For the late cations however, the CASSCF and CASPT2 surfaces are not parallel. The origin of this discrepancy can be ascribed to the double-shell effect, which is far more important for these cations. It was found that incorporat-

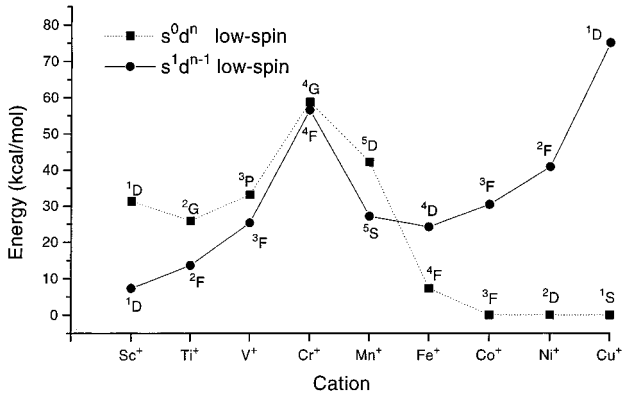

Figure 3. Lowest lying low-spin terms of the first-row transition metal cations (M^+). Experimental energies relative to the ground state.

TABLE 4: CASPT2 Energies Corrected for the Zero-Point Vibrational Energies, Basis Set Superposition Error, and Relativistic effects: Energies (kcal/mol) Relative to the Ground State Asymptote ($M^+ + CH_4$)

	transition state	insertion product
Sc^+	16.7	−6.6
Ti^+	15.3	1.1
V^+	25.7	18.0
Cr^+	54.0	51.5
Mn^+	45.7	33.1
Fe^+	1.84	19.1
Co^+	0.55	11.8
Ni^+	4.64	10.5
Cu^+	25.8	29.3

ing this effect in the CASSCF description (for computational reasons it was not feasible to take this effect into account during the transition state localization) of the wave function already brings the results more in line with the CASPT2 data as collected in Table 4. As this casts some doubt on the conclusions reached for the late cations, our final statements about the stability of the insertion complexes are nevertheless substantiated by considering trends across the row (see next paragraph), by comparison with the experimental results (as discussed in the next section), and by other theoretical studies on the related $HFeC_2H_5^+$ complex by Holthausen et al.[5] and for $HFeCH_3^+$ and H-Co-CH_3^+ by Musaev et al.[2,3]

The general trend across the first row for both the transition state and the insertion product, as depicted in Figure 2, is closely connected to the electronic spectrum of the free metal cation. An analysis of the CASSCF wave function indicates that the electronic structure of the insertion product resembles more an s^1d^{n-1} situation, while the transition state is better described as s^0d^n. As we are dealing with unsaturated complexes, it is logical to compare the relative positions of the lowest lying low-spin states of the s^1d^{n-1} and s^0d^n configurations across the first row. This has been done in Figure 3; the full line connects the position of the lowest s^1d^{n-1} low-spin state and the dashed line the lowest low-spin s^0d^n state of the different free cations. Comparison with Figure 2 immediately reveals a very good similarity between the two figures. For the early metals (Sc^+-Mn^+) the s^1d^{n-1} state is lower than the s^0d^n state, explaining the calculated stability of the insertion product. The late transition metal cations (Fe^+-Cu^+) on the other hand have a low-spin s^0d^n state which is situated below the low-spin s^1d^{n-1} state. For these cations no stable insertion product was found. The crossing between the s^1d^{n-1} and s^0d^n curve occurs between Mn^+ and Fe^+, just as is the case in Figure 2. Furthermore, for Cr^+ Figure 3 predicts that the transition state and insertion product should have more or less the same energy, as indeed is shown in Figure 2.

Comparison with Experiment. An experimental indication for the existence of hydridomethyl complex as an intermediate in the elimination reactions can be obtained from the *branching ratios* for MH^+ and MCH_3^+ formation.[6] From phase space theory calculations it could be concluded that if both reactions proceed through a statistically behaved intermediate, the cross section ratios $\sigma(MH^+)/\sigma(MCH_3^+)$ should lie between 4 and 20. A more direct mechanism, in which not all degrees of freedom equilibrate, gives a branching ratio larger than 20. Sc^+ was found[20] to exhibit a branching ratio ScH^+ to $ScCH_3^+$ of 9, indicating the reaction proceeds via a statistically behaved intermediate. This appears also to be the case for Ti^+ and V^+. Two high-spin states of Ti^+ are observed[21] to have a cross section ratio of 7, while V^+ in its ground state shows[6] a ratio of 4. Although not all states of these cations are found to react statistically, the fact that some states do is a sufficient indication for the existence of a stable intermediate. From Table 4 and Figure 2 it is clear that for Sc^+, Ti^+, and V^+ the experimental indication about the existence of an hydridomethyl intermediate is confirmed by our CASPT2 calculations. As mentioned in the Introduction, a mass spectroscopic indication for a stable $HVCH_3^+$ species is available. This insertion complex was measured to lie 11.8 (± 5.8) kcal/mol above the $V^+(^5D) + CH_4$ asymptote, corresponding quite well to our calculated value of 18.0 kcal/mol

For the Cr^+ reactions the branching ratios do not provide a clear-cut picture for the stability of the insertion complex.[22] $Cr^+(^6S)$ and $Cr^+(^4D, ^4G)$ are characterized by branching ratios of about 25 and 30, respectively. These numbers suggest a mixed behavior: the intermediate that is formed in the course of the reaction is not fully equilibrated. To some extent our calculations confirm this observation, since the energy difference between the transition state and the intermediate (Table 3) amounts only to 2.5 kcal/mol. This small energy barrier gives rise to a short-lived intermediate, for which a complete equilibration among all degrees of freedom is probably impossible.

Branching ratios for the $^{23}Fe^+$ and $^{24}Co^+$ reactions with methane point to an CH_3 elimination that is more than 30 (even reaching 40 for Fe^+) times more efficient. In agreement with our calculations these values must be interpreted to mean that no statistically behaved intermediate plays any active role in these reactions. It should be noted that in our previous study a stable linear quintet $HCoCH_3^+$ was characterized. However, this structure is not likely to participate in the thermal reactions of Co^+ with CH_4 because of its high energetic position with respect to the reactants. Also guided-beam experiments do not proceed through this quintet intermediate because the ^3F ground state of Co^+ (for which these experiments were conducted) reacts in a diabatic fashion due to the large kinetic energies. For Co^+ as well as for Fe^+ previous theoretical[2,3] and experimental[23,24] studies could not locate a low-spin minimum on the potential energy surface and therefore agree with our CASPT2 calculations.

As mentioned in the Introduction the *H_2 elimination* is the dominant process for the reaction of the early metals with methane. At first sight it might be tempting to ascribe this feature to the stability of the insertion complexes. This seems however not to be the case, as can be deduced from the reactions of the chromium and manganese cation. From our calculations and from the experimental branching ratios the insertion complex of Cr^+ is not very stable,[22] while for Mn^+ the insertion complex is predicted to be quite stable. Experimentally the H_2 elimination is a dominant process for Cr^+, while for Mn^+ it is not.[1] We must therefore conclude that some other effect is responsible for the observed reactivity pattern.

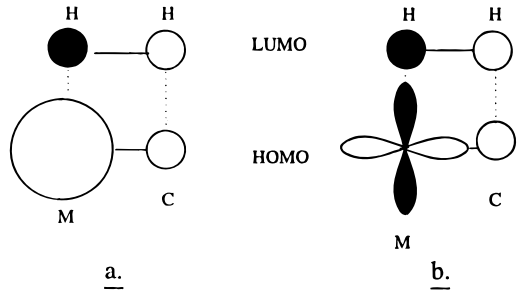

Figure 4. Schematic representation of the LUMO (H_2) + HOMO (M−C) interactions for the reverse reaction $H_2 + MCH_2^+ \rightarrow HMCH_3^+$. The M−L bonds established either entirely by means of the metal 4s orbital (a) or entirely by the metal 3d orbitals (b).

According to Goddard et al.[25] the 4s and 3d participation in the M−L bonds must be thought of as the crucial factor controlling the effectiveness of the H_2 elimination. On the basis of their GVB calculations on some prototype complexes these authors argued that if the metal ligand bonding is covalent and if it involves the 4s orbital of the cation, the H_2 elimination should be regarded as a symmetry-forbidden $2_s + 2_s$ reaction. If the M−L bond has a substantial 3d contribution, the energy barrier in the exit channel was calculated to decrease. This result can also be understood in terms of the frontier orbital approach. Indeed, the HOMO and the LUMO of the M−C bond will have a larger overlap with the LUMO and the HOMO, respectively, of the H_2 molecule when the M−C and M−H bonds have a larger 3d participation (Figure 4). Our calculations confirm this picture, as can be inferred from a Mulliken population analysis (Table 2) of the CASSCF wave function. The 4s population remains almost constant at about 0.5*e* for Sc^+ to Cr^+, while for Mn^+ to Cu^+ it amounts to as much as 0.8*e*. This corresponds to a dramatic increase from Cr^+ to Mn^+. Although the $HMnCH_3^+$ complex is a minimum on the potential energy surface, its large 4s participation in the M−C bond appears to more crucial for understanding its ability to eliminate H_2.

Conclusion

The picture that emerges from our ab initio calculations can be summarized in the following way. On the right side of the first transition row the 4s orbital has a larger radial extent with respect to the 3d shell. For the late cations of this row the M−H bonding is almost exclusively derived by means of the 4s orbital. Due to the directional character of the interacting sp^3 orbital of the methyl group, the M−C bond results mainly from an interaction with the 3d orbitals. The metal cations at the left side of the row, on the other hand, form bonds with the hydrogen and methyl ligands by using a larger involvement of the 3d orbitals. This is the consequence of a more similar radial extent of the 4s and 3d orbitals for these elements, which makes an sd hybridization more feasible. In particular our calculations indicate that the 3d participation in the M−H bond increases notably from the right to the left in the row. As the 3d shell is more shielded by the 4s orbital for the late metals, the M−C bond becomes weaker, as is witnessed by the occupation numbers of the bonding and antibonding orbital for this bond.

An analysis of the wave function reveals that the transition states resemble more closely a s^0d^n configuration, whereas the insertion complexes possess a larger s population. Therefore, the stability of the insertion complexes is found to correlate with the relative position of the lowest low-spin s^1d^{n-1} state with respect to the lowest low-spin s^0d^n state for the free cation. Both the weakening of the M−C bond and the fact that the 3d contraction across the row favors an s^0d^n ground state (Figure 3) cause the insertion products for the late transition metal cations to be unstable. Our CASPT2 calculations predict stable hydridomethyl complexes for Sc^+, Ti^+, V^+, and Mn^+.

These theoretical results explain the specific trends in the reactivity of the first-row singly charged transition metal cations with methane. The cross section ratios indicate statistically behaved intermediate structures for Sc^+, Ti^+, and V^+. For Cr^+ a mixed behavior is observed, which is confirmed by the fact that only a slightly stable insertion complex was found on the potential energy surface. Branching ratios measured for Fe^+ and Co^+ suggest a direct reaction mechanism for the experimentally observed elimination reactions. In agreement with these observations, our calculations could not locate a low-spin stable $HMCH_3^+$ structure for these two metals. Finally, the H_2 elimination was found to relate closely to the 4s participation in the M−L bonds. The dominance of this elimination, as experimentally measured for Sc^+ to Cr^+, is reflected in the calculated reduction of the occupation of the 4s orbital in the corresponding insertion complexes. A very significant increase for the 4s population was noticed to occur between Cr^+ and Mn^+.

References and Notes

(1) Armentrout, P. B.; Beauchamp, J. L. *Acc. Chem. Res.* **1989**, *22*, 315.

(2) Musaev, D. G.; Morokuma, K.; Koga, N.; Nguyen, K. A.; Gordon, M. S.; Cundari, T.T. *J. Phys. Chem.* **1993**, *97*, 11435.

(3) Musaev, D. G.; Morokuma, K. *J. Chem. Phys.* **1994**, *101*, 10697.

(4) Hendrickx, M.; Ceulemans, M.; Vanquickenborne, L. *Chem. Phys. Lett.* **1995**, *257*, 8.

(5) (a) Holthausen, M. C.; Fiedler, A.; Schwarz, H.; Koch, W. *Angew. Chem.* **1995**, 107, 2430. (b) Holthausen, M. C.; Fiedler A.; Schwarz, H.; Koch, W. *J. Phys. Chem.* **1996**, *100*, 6236.

(6) Aristov, N.; Armentrout, P. B. *J. Phys. Chem.* **1987**, *91*, 6178.

(7) Blomberg, M. R. A.; Siegbahn P. E. M.; Svenson, M. *J. Phys. Chem.* **1994**, *98*, 2062.

(8) Andersson, K.; Malmqvist, P.-A.; Roos, B. O.; Sadlej, A. J.; Wolinski, K. *J. Phys. Chem.* **1990**, *94*, 5483.

(9) Andersson, K.; Malmqvist, P.-A.; Roos, B. O. *J. Chem. Phys.* **1992**, *96*, 1218.

(10) Pou-Amerigo, R.; Merchan M.; Nebot-Gil, I.; Malmqvist, P.-A.; Roos, B. O. *J. Chem. Phys.* **1994**, *101*, 4893.

(11) Pierloot, K.; Dumez, B.; Widmark, P.-O.; Roos, B. O. *Theor. Chim. Acta* **1995**, *90*, 87

(12) *MOLCAS* version 3; Anderson, K., Blomberg, M. R. A., Fulscher, M. P., Kello, V., Lindh, R., Malmqvist, P.-A., Noga, J., Olsen, J., Roos, B. O., Sadlej, A. J., Siegbahn, P. E. M., Urban, M., Widmark, P.-O., Eds.; University of Lund: Sweden, 1994.

(13) *GAMESS*: Schmidt, M. W.; Baldridge, K. K.; Boatz, J. A.; Jensen, J. H.; Koseki, M. S.; Gordon, M. S.; Nguyen, K. A.; Windus, T. L.; Elbert, S. T. *QCPE Bull.* **1990**, *10*, 52.

(14) Wachters, A. J. H. *J. Chem. Phys.* **1970**, *52*, 1033.

(15) Dunning, T. H. *J. Chem. Phys.* **1970**, *53*, 2823. Huzinaga, S. *J. Chem. Phys.* **1965**, *42*, 1293.

(16) Schilling, J. B.; Goddard, W. A., III; Beauchamp, J. L. *J. Am. Chem. Soc.* **1986**, *108*, 582.

(17) Bauschlicher, C. W., Jr; Langhoff, S. R.; Partridge, H.; Barnes, L. A. *J. Chem. Phys.* **1989**, *91*, 2399.

(18) Rosi, M.; Bauschlicher, C. W., Jr.; Langhoff, S. R.; Partridge, H. *J. Phys. Chem.* **1990**, *94*, 8656.

(19) Holthausen, M. C.; Heinemann, C.; Cornehl, H. H.; Koch, W.; Schwarz, H. *J. Chem. Phys.* **1995**, *102*, 4931.

(20) Sunderlin, L. S.; Armentrout, P. B. *J. Am. Chem. Soc.* **1989**, *111*, 3845.

(21) Sunderlin, L. S.; Armentrout, P. B. *J. Phys. Chem.* **1988**, *92*, 1209.

(22) Georgiadis, R.; Armentrout, P. B. *J. Phys. Chem.* **1988**, *92*, 7067.

(23) Haynes, C. L.; Chen, Y.-M.; Armentrout, P. B. *J. Phys. Chem.* **1996**, *100*, 111.

(24) Haynes, C. L.; Chen, Y.-M.; Armentrout, P. B. *J. Phys. Chem.* **1995**, *99*, 9110.

(25) Steigerwald, M. L.; Goddard, W. A., III *J. Am. Chem. Soc.* **1984**, *106*, 308.